 doi:10.20944/preprints201907.0140.v1

Article

Pathway-Focused Gene Interaction Analysis Reveals the Regulation of TGFβ, Pentose Phosphate and Antioxidant Defense System by Placental Growth Factor in Retinal Endothelial Cell Functions: Implication in Diabetic Retinopathy

Hu Huang [1,*], Madhu Sudhana Saddala [1], Anton Lennikov [1], Anthony Mukwaya [2] and Lijuan Fan[1]

[1] Mason Eye Institute, University of Missouri, Columbia, Missouri, United States of America
[2] Department of Ophthalmology, Institute for Clinical and Experimental Medicine, Faculty of Health Sciences, Linköping University, Linköping, Sweden
* Correspondence: huangh1@missouri.edu; Tel.: +1-573-882-9899 (H.H.)

Abstract:

Placental growth factor (PlGF or PGF) is a member of the VEGF family, which is known to play a critical role in pathological angiogenesis, inflammation, and endothelial cell barrier function. However, the molecular mechanisms by which PlGF mediates its effects in non-proliferative diabetic retinopathy (DR) remain elusive. In this study, we performed transcriptome-wide profiling of differential gene expression for human retinal endothelial cells (HRECs) treated with PlGF antibody. The effect of antibody treatment on the samples was validated using trans-endothelial electric resistance (TEER), and western blot. A total of 3760 genes (1750 upregulated and 2010 downregulated) were found to be differentially expressed between the control and PlGF antibody treatment group. These differentially expressed genes (DEGs) were used for gene ontology and enrichment analysis to identify gene function, signal pathway, and interaction networks. The gene ontology results revealed that catalytic activity (GO:0003824) of molecular function, cell (GO:0005623) of the cellular component, and cellular process (GO:0009987) were among the most enriched biological processes. Pathways such as TGF-β, VEGF-VEGFR2, p53, apoptosis, pentose phosphate pathway, and ubiquitin-proteasome pathway, were among the most enriched, and TGF-β1 was identified as a primary upstream regulator. These data provide new insights into the underlying molecular mechanisms of PlGF in mediating biological functions, in relation to DR.

Keywords: PlGF; PGF; blood-retinal barrier; RNA Seq; HREC; gene ontology; fastQC; Trimmomatic; KEGG; pentose phosphate pathway; TGF-β

1. Introduction

Diabetic Retinopathy (DR) is the most common complication of diabetes and the leading cause of visual impairment in the working-age adult population worldwide [1]. Increased glucose levels can lead to microvascular damage in the retina. However, the mechanism by which hyperglycemia initiates retinal blood vessel damage in retinopathy remains elusive. It is well documented that oxidative stress and inflammation play a vital role in this process, ultimately resulting in the breakdown of the blood-retinal barrier (BRB) [2]. An impaired BRB can further progress into augmented vascular retinal permeability and irregular growth of new blood vessels, instigating moderate to severe vision loss. When DR progresses into further advanced stages, vitreous hemorrhages can occur and result in retinal detachment and fibrovascular contraction, further advancing vision loss, and eventually leading to blindness [3].

Preprints (www.preprints.org) | NOT PEER-REVIEWED | Posted: 10 July 2019 doi:10.20944/preprints201907.0140.v1

The identification of vascular endothelial growth factor (VEGF) as a major stimulus for proliferative diabetic retinopathy (PDR) led to the development of anti-VEGF therapies, which have improved the clinical management of this condition. However, repeated anti-VEGF therapy in severe PDR patients can lead to the formation of fibrovascular membranes (FVM) and tractional retinal detachment, which can cause severe vitreoretinal traction and hemorrhage [4]. A study in the literature has also suggested that long-term intravitreal (ITV) anti-VEGF injection may have deleterious effects on the neuronal cells, based on the survival and maintenance function of VEGF [5]. Thus, there is a clear need for alternative therapies for DR, especially for the non- or poor-responders to the current standard of care, with the potential to reduce the risk of treatment-related sequelaes. Indeed, other crucial angiogenic growth factors are likely involved in this condition [6], which could serve as additional or even alternative targets for therapy. Cumulative evidence supports the pathogenic role of placental growth factor (PlGF), which is a member of the VEGF family and was first described from a human placental cDNA library in 1991 [7,8]. PlGF is expressed by a wide variety of cell types, including endothelial cells (ECs) and retinal pigment epithelial cells (RPEs) in response to hypoxia [9]. PlGF is a homolog of VEGF and binds to fms-like tyrosine kinase-1 (VEGFR-1; also known as FLT1) and soluble VEGFR-1, a circulating form of VEGFR-1 that lacks the transmembrane and intracellular domains. Activation of FLT1 by PlGF augments the effects of VEGF-VEGFR2 signaling, suggesting synergistic effects of PlGF and VEGF. PlGF can also form heterodimers with VEGF [10] and exerts a strong effect on blood vessel growth and maturation. Further, PIGF has direct proangiogenic effects on ECs [11]. Previously, we reported that deleting PlGF decreased expression of diabetes-activated hypoxia-inducible factor (HIF)1α in the mouse retina. We also described changes in the VEGF pathway including expression of HIF1α, VEGF, VEGFR1–3, and levels of phospho (p)-VEGFR1, p-VEGFR2, and p–endothelial nitric oxide synthase in the retinas of diabetic PlGF$^{-/-}$ mice [12].

Despite the advances made, the biological function of PIGF and associated mechanisms are less well understood than those of its homolog VEGF. In order to address this gap, we sought to perform a comparative transcriptomic analysis between the PlGF antibody (ab) treatment and the Phosphate-Buffered Saline (PBS) control in the primary human retinal endothelial cell (HREC). We identified transcriptome and pathways that are regulated by PlGF. In one recent study (manuscript under review), we report some preliminary results, including several signaling pathways that are pertinent to EC barrier functions: VEGF receptor signal, pentose phosphate pathway, and anti-oxidation systems. In the present study, we provide a thorough report about the differentially expressed genes (DEGs) in HREC with the presence and absence of PlGF signaling and highlight several signaling pathways regulated by PlGF. Notably, the expression levels of many genes involved in the TGF-β signaling pathway, which acts as a primary regulator of many other identified genes and pathways, are altered in the PlGF ab treatment relative to the PBS control.

2. Materials and Methods

Primary human retinal endothelial cell (HREC) culture

Primary human retinal endothelial cells (HRECs) were bought from Cell Systems (Cat#: ACBR1 181, Kirkland, WA). HRECs were seeded on fibronectin-coated (10 μg/ml, overnight, 33016015, Gibco) plastic culture vessels and grown using the EBM2-MV medium (Cat#: cc-4176, Lonza, Walkersville, MD) supplemented with 10% fetal bovine serum (FBS), 1% of penicillin/streptomycin (P/S), and EGM MV Singlequots growth supplement kit (Cat#: cc-4147, Lonza). Cells were used during passage 5 to 6.

Cell treatments

At 80% confluence, the culture media was replaced with fresh media containing mouse anti-PlGF antibody (5D11D4), (25 μg/ml) and HRECs were collected 48 hours after the start of the incubation. PBS treated cells were used as a negative control.

Sample validation

Preprints (www.preprints.org) | NOT PEER-REVIEWED | Posted: 10 July 2019 doi:10.20944/preprints201907.0140.v1

Trans-endothelial electrical resistance (TEER) measurement by Electric Cell-Substrate Impedance Sensing (ECIS) system

Primary HRECs were seeded onto an 8-well ECIS array, cultured, and treated with anti-PlGF antibody or recombinant human (rh) PlGF as described above. For the antibody effects validation, rh PlGF protein (Cat#: 264-PGB-010/CF, R&D Systems, Minneapolis, MN), (0.5 µl; 100 ng/ml) was used as a positive control. TEER was monitored with the ECIS system (Applied Biophysics, Troy, NY) in real time. The changes in TEER were automatic monitored every 600s at 4 kHz AC frequency and recorded on the ECIS software. The embedded mathematical model of impedance change was used to calculate the TEER (Ω/cm^2), a measure of cell-to-cell barrier and cell-to-substratum function [13].

Western blots (WB) analysis

WB was performed as previously described [14,15]. HRECs were grown in the 6-well plates with the conditions and treatments as described above. Next, the experimental endpoint cells were washed with cold D-PBS three times, detached with a cell scraper, and collected by centrifugation. The harvested cell pellets were sonicated in cold RIPA buffer containing FAST protease inhibitor (Cat#: S8830, Sigma, St Louis, MO). Protein concentration was determined using the DC™ Protein Assay kit (Bio-Rad, Hercules, and CA) and/or Qubit 4 Fluorometer. Then, 30-50 µg of total protein per lane was separated by SDS-PAGE (4-20% polyacrylamide gel) prior to electrophoretic transfer to 0.45 µm pore size nitrocellulose membranes. The membranes were blocked with 5% non-fat milk (Bio-Rad) at room temperature for 1 hr and then incubated overnight at 4 ºC with the following primary antibodies: anti-VE-Cadherin (1:1,000, Cat#: 5012896, Thermo Fisher Scientific), anti-G6PD (1:500, Cat#: MA5-15918, Thermo Fisher Scientific, Halethorpe, MD), and anti-β-actin (1:1000, Cat#: PA5-16914, Cell Signaling, Danvers, MA). After washing with PBS-T buffer, the blots were incubated with horseradish peroxidase (HRP)-conjugated 1:1000 secondary antibody in 5% milk (Goat anti-Rabbit IgG, Cat#: 170-6515; Goat anti-Mouse IgG Cat#: 172-1011; Goat anti-Rat IgG 5204-2504 Bio-Rad) for 1 h at room temperature (RT). Signals were developed with enhanced chemiluminescence (ECL) using a Super Signal West Pico kit (Thermo Fisher) and detected using ImageQuant LAS500 (GE Healthcare Life Science, Pittsburgh, PA, USA).

RNA extraction

Forty-eight hours after treatment, the cells were washed with PBS, and total RNA was extracted using the Qiagen mini RNA preparation kit (Qiagen) according to the manufacturer's protocol. RNA concentration was determined using a NanoDrop spectrophotometer (Thermo Scientific). RNA quality was determined using the Agilent bioanalyzer 2100 (Agilent Technologies). The analysis showed clear, defined 28s and 18s rRNA peaks, an indication of high-quality RNA. Volume, concentration, and RIN values of the RNA samples are presented in Table 1. RIN value ≥ 8 was set as the cut-off for sample inclusion for downstream processing for RNA sequencing analysis.

RNA sequencing

RNA samples were submitted to Novogene Leading Edge Genomic Services & Solutions, California, USA, for sample preparation and sequencing. The samples were first DNase-treated and assessed for total RNA quality using the Agilent 2100 Bioanalyzer, followed by 2 rounds of polyadenylate positive (poly A+) selection and conversion to cDNA. RNA sequencing was performed on the Illumina HiSeq 2500 using the latest versions of sequencing reagents and flow cells, providing up to 300 GB of sequence information per flow cell. TruSeq library generation kits were used according to the manufacturer's instructions (Illumina). Library construction consisted of random fragmentation of the poly A+ mRNA, followed by cDNA production using random primers. The ends of the cDNA were repaired, A-tailed, and adaptors ligated for indexing (up to 12 different barcodes per lane) during the sequencing run. The cDNA libraries were quantitated using qPCR in a Roche LightCycler 480 with the Kapa Biosystems kit for library quantitation (Kapa Biosystems) prior to cluster generation. Clusters were generated to yield approximately 725K–825K clusters/mm2. Cluster density and quality were determined during the run after the first base addition parameters were

Preprints (www.preprints.org) | NOT PEER-REVIEWED | Posted: 10 July 2019 doi:10.20944/preprints201907.0140.v1

assessed. Paired-end 2 × 50 bp sequencing runs were performed to align the cDNA sequences to the reference genome mouse mm10. Approximately 15 million paired 50 bp reads were obtained per sample. The raw fastq reads were trimmed for adapters and pre-processed to remove low-quality reads using Trimmomatic v. 0.36 with default parameter setting for Illumina paired-end reads, to retain more than 97% of good quality reads in each stage. After adapter removal, the quality of each paired-end sequence file was evaluated using FastQC analysis http://www.bioinformatics.babraham.ac.uk/projects/fastqc/ based on the following parameters: 1) Distribution of quality score (Phred score) per base, 2) Distribution of quality scores of the raw sequences, 3) Distribution of duplicated reads, and 4) GC content (%) distribution of the raw sequences. For each sample, trimmed short reads were mapped to the human genome (TopHat and Cufflinks), resulting in 10–95 million mapped reads per sample. We performed quality-control or global analysis (quality of the model fitting) of the cufflinks data by using the CummeRbund R package (http://compbio.mit.edu/cummeRbund/).

RNA-Seq bioinformatics analysis

The raw data were evaluated for reads quality before and after pre-processing using FastQC software: (https://www.bioinformatics.babraham.ac.uk/projects/fastqc/). The reads were processed to remove adapters and ambiguous quality reads using the Trimmomatic-0.36 tool [16] with trimming of bases from 3′ and 5′ end, maintaining the Phred-score ≤ 30. The human genome was downloaded from the National Centre for Biotechnology Information (NCBI) genome (https://www.ncbi.nlm.nih.gov/genome/?term=human) for reference-based assembly. We mapped all the datasets onto the human genome reference sequence GRCh38 using TopHat2.0.9 (http://ccb.jhu.edu/software/tophat/index.shtml). The expression levels were transformed into fragments per kilobase of exon per million mapped fragments (FPKM). We identified DEGs that satisfy the significance expressed as q-value representing FDR-adjusted P value < 0.05 by using Cufflinks 2.1.1 (http://cufflinks.cbcb.umd.edu). The Bioconductor tool with CummeRbund package was employed to analyze differential expression analysis in the assembled transcriptome (http://compbio.mit.edu/cummeRbund/manual_2_0.html). Finally, both control and PlGF ab treated comparison transcript counts (matrix file) were used for differential gene expression using the CummeRbund package of Bioconductor with primary parameters such as FDR (false discovery rate), logFC (log fold-change), logCPM (log counts per million), and p-value. Unigenes with adjusted q-values of less than 0.05 ($p<0.05$) and the fold change of more than 2 ($logFC>2$) were considered as significantly differentially expressed genes.

Functional annotation

Gene ontology (GO) Enrichment Analysis (http://geneontology.org/page/go-enrichment-analysis) and DAVID annotation (https://david.ncifcrf.gov/) were used for functional annotation and pathways analysis. An adjusted EASE (Expression Analysis Systemic Explore Score) score of 0.05 and threshold count of >2 genes were employed. Benjamin–Hochberg multiple testing correction was applied to the p-values. GO terms with FDR $q<0.05$ were considered significantly enriched within the gene set [17] [18].

Gene-gene network analysis

We performed protein-protein network analysis for all DEGs using the STRING 10.5 database (https://string-db.org/). This is calculated in a variety of classification systems (Gene Ontology, KEGG, Pfam and InterPro), and used the Fisher's exact test followed by a correction for multiple testing [18,19].

Statistical analysis

All numeric values were expressed as the mean ± standard deviation (SD) for the respective groups. Statistical analyses were performed using the Trinity software (https://github.com/trinityrnaseq/trinityrnaseq/wiki). Student t-tests and Benjamin–Hochberg

Preprints (www.preprints.org) | NOT PEER-REVIEWED | Posted: 10 July 2019 doi:10.20944/preprints201907.0140.v1

corrections (FDR) were also used in the analyses. A p-value of less than 0.05 was considered significant.

3. Results

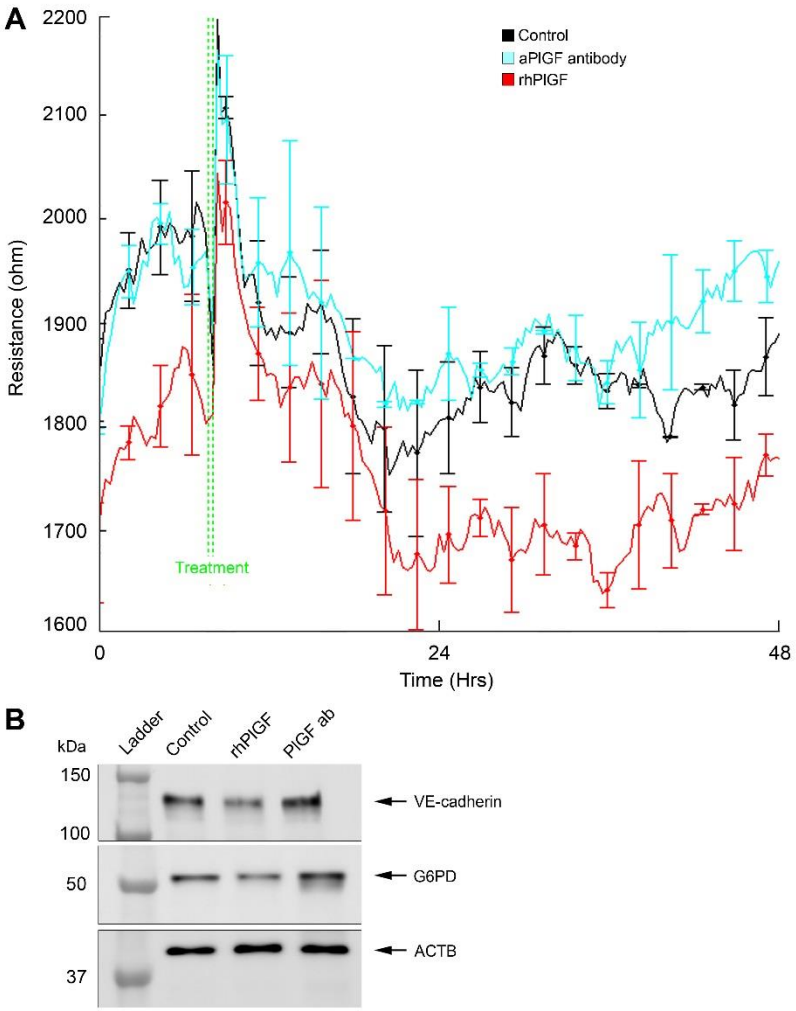

Figure 1. Trans-endothelial electric resistance (TEER) values of HRECs treated with PBS (Control), rhPlGF 100 ng/ml, and anti-PlGF antibody 25 μg/ml for the course of 48 hours (**A**). Western blot analysis of VE-cadherin and G6PD in protein samples acquitted from HREC cultures after 48 hours incubation with the same treatments at the end of the 48 hour period.

3.1. Effects of PlGF antibody and recombinant PlGF on HREC resistance, G6PD, and VE-Cadherin

By using PlGF antibody and recombinant PlGF, we recently demonstrated that PlGF acts as a negative regulator of EC barrier function through suppression of glucose-6-phosphate dehydrogenase (G6PD) and barrier-forming proteins, such as VE-cadherin (manuscript under review). In agreement with the previous observations, in our new experimental settings, we found that the PlGF antibody boosted, but recombinant PlGF reduced HREC resistance, which was evaluated using TEER measurement by the ECIS system: effective separation in cell monolayer resistance values over time was observed between the control, anti-PlGF antibody, and rhPlGF protein (Figure 1A). With the increased resistance of αPlGF antibody-treated cells and decreased resistance of rhPlGF treated cells, the effects were monitored at up to 48 hours' time point where protein and RNA samples were collected. The changes in the protein levels of CDH5 (VE-cadherin)

Preprints (www.preprints.org) | NOT PEER-REVIEWED | Posted: 10 July 2019 doi:10.20944/preprints201907.0140.v1

and G6PD were validated by WB analysis (Figure 1B). The expression levels of VE-cadherin and G6PD were upregulated by αPlGF antibody treatment and downregulated in rhPlGF treated cells. The HREC RNA samples were then used for sequencing and bioinformatics analyses.

3.2. RNA sequencing

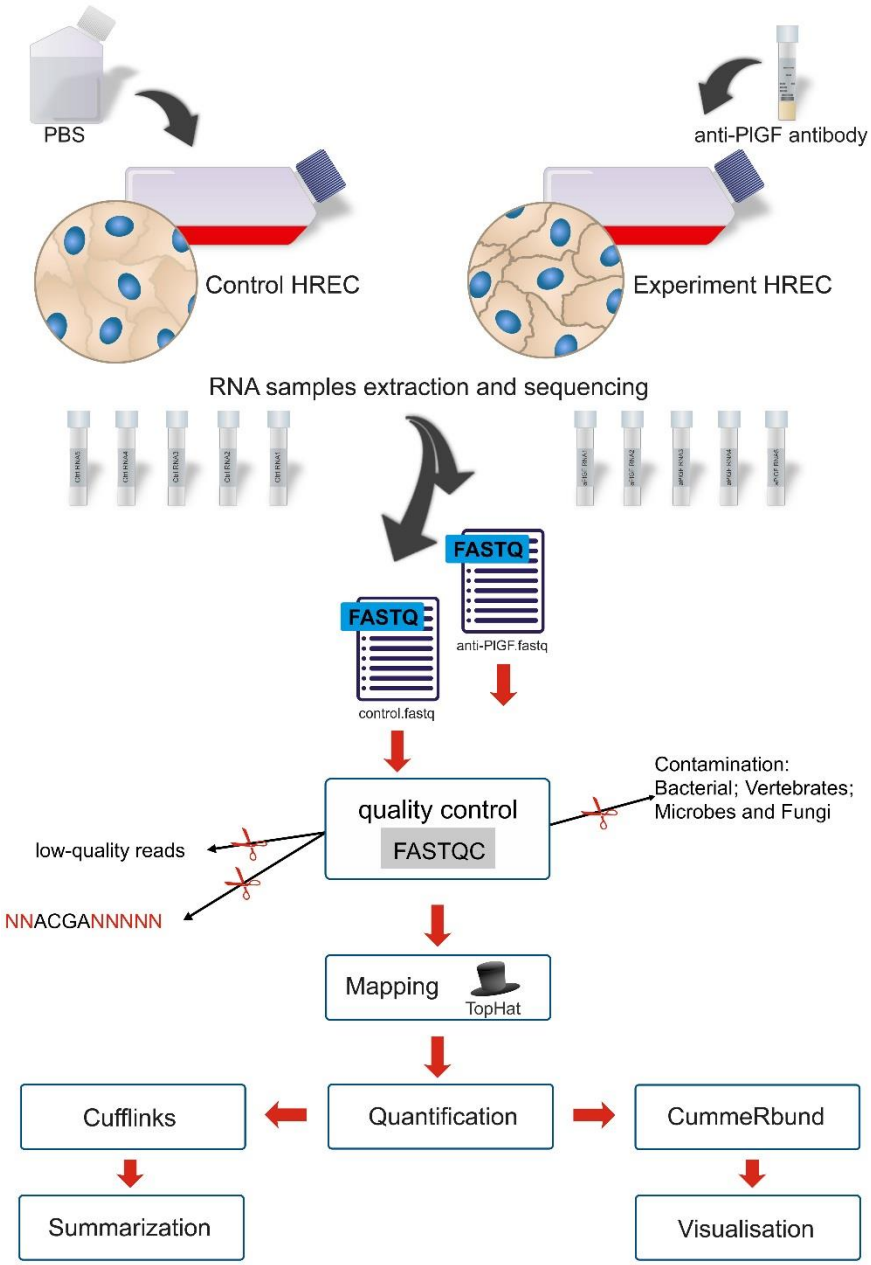

Figure 2. Present study workflow pipeline. The pipeline of RNA-Seq analysis uses TopHat to align RNA-seq reads, Cufflinks to assemble and estimate the relative transcript abundance and cuffmerge for Cufflinks assemblies, and CummeRbund for visualization and the statistical analysis.

Preprints (www.preprints.org) | NOT PEER-REVIEWED | Posted: 10 July 2019 doi:10.20944/preprints201907.0140.v1

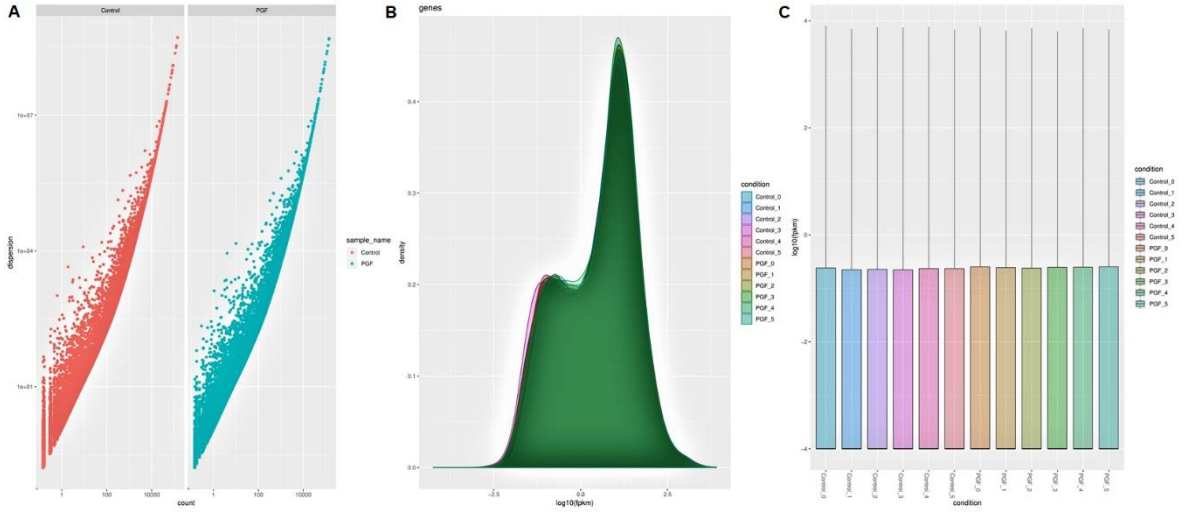

Figure 3. The quality of a higher number of differentially expressed genes representation. **A**. Model fitting dispersion plot. **B**. Density plot **C**. Box plot.

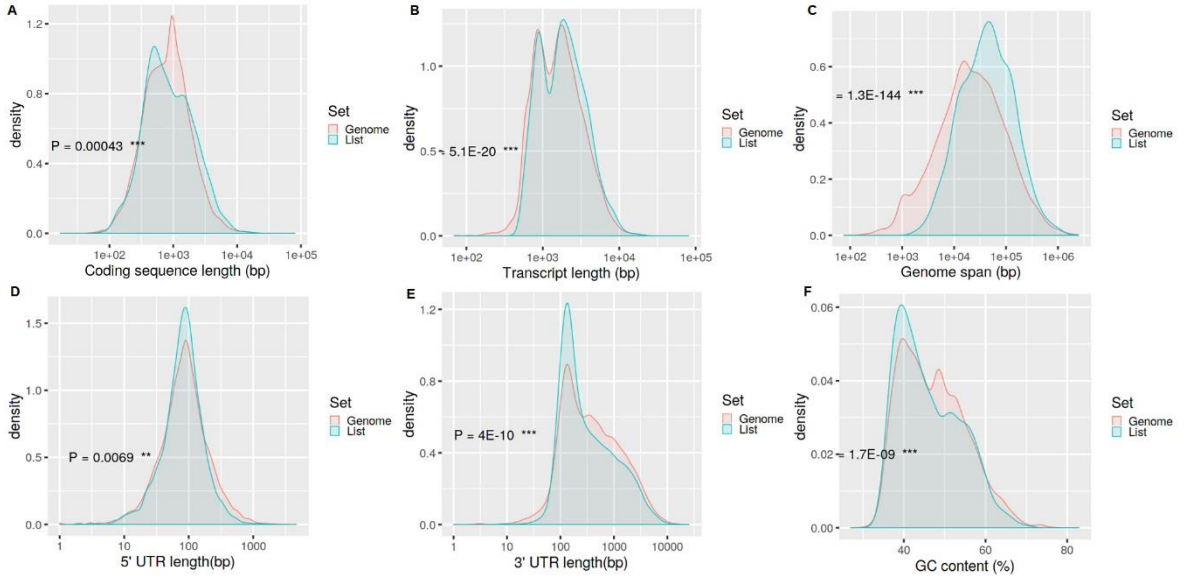

Figure 4. Raw sequencing component analysis on the reference genome. **A**. Coding sequence length(bp) **B**. Transcript length(bp) **C**. Genome span(bp), **D**. 5′ UTR length(bp) **E**. 3′ UTR length(bp) **F**. Percentage of GC content in DEGs.

Preprints (www.preprints.org) | NOT PEER-REVIEWED | Posted: 10 July 2019 doi:10.20944/preprints201907.0140.v1

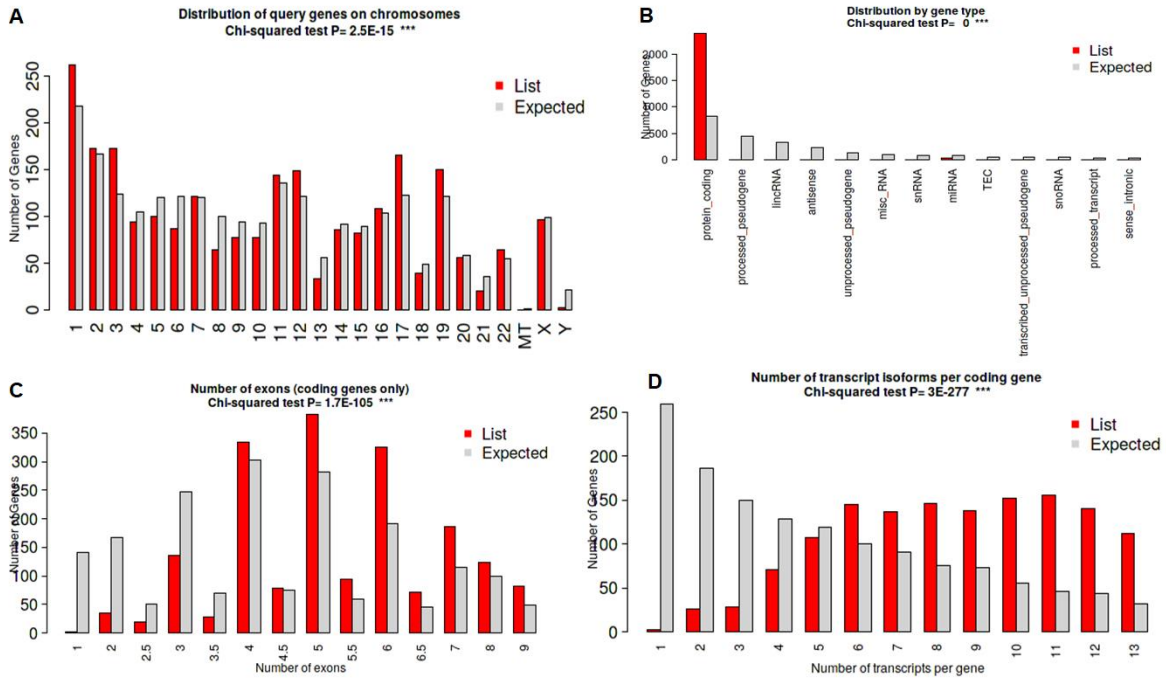

Figure 5. Distribution of DEGs sequencing component analysis **A**. Distribution of DEGs chromosomes **B**. Distribution of gene type **C**. Number of exons (coding genes) **D**. Number of transcript isoforms per coding gene.

Preprints (www.preprints.org) | NOT PEER-REVIEWED | Posted: 10 July 2019 doi:10.20944/preprints201907.0140.v1

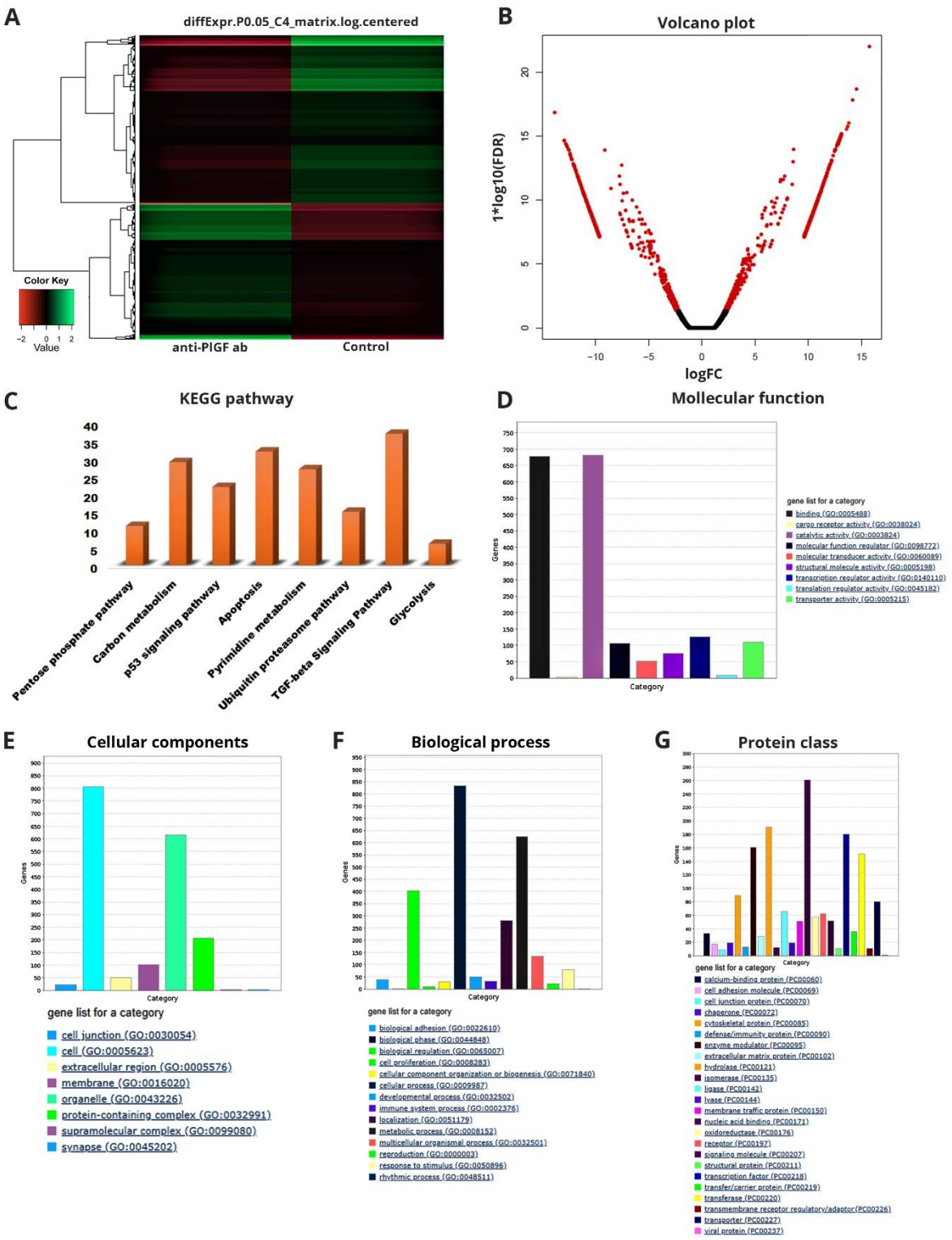

Figure 6. Gene expression profile in PlGF ab treated group relative to the control. **A**. The differentially expressed genes are plotted in the form of a heat map, where red color represents down-regulated, while green color represents up-regulated (logFC±2; p-values=0.05). The dendrogram provides a hierarchical clustering. **B**. Volcano plot represented by significantly up and down-regulated gene based on the logFC and log10(FDR). **C**. KEGG (Kyoto Encyclopedia of Genes and Genomes) pathways. The differentially expressed genes involved in pentose phosphate pathway, carbon metabolism pathway, p53 signaling pathway, apoptosis pathway, pyrimidine metabolism pathway, ubiquitin-proteasome pathway, TGFβ signaling pathway and glycolysis pathway **D**. Molecular function (MF) **E**. Cellular component (CC) **F**. Biological process (BP) **G**. Protein class of DEGs.

 doi:10.20944/preprints201907.0140.v1

The RNA-Seq approach was designed to provide an in-depth investigation of the transcriptome-wide differential gene expression profiles and therapeutic target pathway genes predictions. The workflow of the current study is represented in Figure 2. The cuffdiff results file was statistically analyzed and visualized using the cummeRbund package. The quality of the model fitting dispersion plot (Figure 3A) showed the highest number of differentially expressed genes (DEGs). In addition, we calculated the distributions of FPKM (Fragments Per Kilobase of transcript per Million) scores across samples using the Density plot and Box plot, respectively (Figure 3B and C). The coding sequence length (bp), transcript length (bp), genome span (bp), 5′ UTR length(bp), 3′ UTR length(bp), and percentage of the GC content of DEGs were predicted (Figure 4). In addition, the distribution of DEGs was predicted based on the human chromosomes, distribution of gene type, number of exons (coding genes), and number of transcript isoforms per coding gene (Figure 5). We identified 53808 significant transcripts in total from the datasets. Among them, a total of 3275 differentially expressed genes (1750 up-regulated and 2010 down-regulated genes) that satisfy *q*-value (FDR-corrected p-value) < 0.05 and fold change ≥ ±2.0, were identified in the PlGF ab treated group relative to the control. A hierarchical clustering heatmap and volcano plots were generated to represent the up- and downregulated genes (Figure 6A and B). These DEGs were used for further gene ontology and functional pathway analysis.

3.2.1 Functional annotation

DEGs were used for GO enrichment analysis using the DAVID annotation tool [20] with the complete human genome as the background. The following GO terms were enriched: molecular function (MF), biological process (BP), cellular component (CC), and protein classes (PC). Most of the DEGs were found to be involved in several molecular functions, such as binding (GO:0005488), catalytic activity (GO:0003824), molecular function regulator (GO:0098772), structural molecule activity (GO:0005198), transcription regulator activity (GO:0140110), and transporter activity (GO:0005215). Among these molecular functions, DEGs were most involved in binding (GO:0005488), catalytic activity (GO:0003824), and translation regulator activity (GO:0045182), respectively (Figure 6D). The DEGs were also involved in various cellular components i.e., cell junction (GO:0030054), cell (GO:0005623), membrane (GO:0016020), protein-containing complex (GO:0032991), and synapse (GO:0045202). Among these cellular components, the DEGs were most involved in the cell (GO:0005623), organelle (GO:0043226), and protein-containing complex (GO:0032991), respectively (Figure 6E). The DEGs were also involved in various biological processes i.e., biological adhesion (GO:0022610), biological regulation (GO:0065007), cellular component organization or biogenesis (GO:0071840), cellular process (GO:0009987), immune system process (GO:0002376), and metabolic process (GO:0008152) but the DEGs were most involved in biological regulation (GO:0065007), cellular processes (GO:0009987), and metabolic process (GO:0008152), respectively (Figure 6F). The DEGs were also classified into to several protein classes such as calcium-binding protein (PC00060), cell adhesion molecule (PC00069), cell junction protein (PC00070), chaperone (PC00072), defense/immunity protein (PC00090), extracellular matrix protein (PC00102), nucleic acid binding (PC00171), signaling molecule (PC00207), transfer/carrier protein (PC00219), transmembrane receptor regulatory/adaptor protein (PC00226), and transporter (PC00227), respectively. Most of the DEGs are classified as nucleic acid binding (PC00171), hydrolase (PC00121), transcription factor (PC00218), and enzyme modulator (PC00095) (Figure 6G).

The gene ontology results revealed that the 36.9% of the genes were involved in binding (GO:0005488), 37.1% of genes were involved in catalytic activity (GO:0003824), and 6.9% of genes were involved in transcription regulator activity (GO:0140110) of molecular functions. A total of 44.5% of genes participated in the cell (GO:0005623), 34.0% of genes participated in the organelle (GO:0043226), and 11.4% of genes participated in the protein-containing complex (GO:0032991) of cellular components. A total of 32.8% of the genes were involved in cellular processes (GO:0009987), 24.6% of genes were involved in the metabolic process (GO:0008152), 15.9% of genes were involved in biological regulation (GO:0065007), and 11.0% of genes were involved in localization (GO:0051179) of biological processes. Finally, 16.2% of genes belonged to nucleic acid binding (PC00171), 11.9% of

Preprints (www.preprints.org) | NOT PEER-REVIEWED | Posted: 10 July 2019 doi:10.20944/preprints201907.0140.v1

299 genes belonged to hydrolase (PC00121), 11.2% of genes belonged to the transcription factor
300 (PC00218), 10.0% of genes belonged to enzyme modulator (PC00095), 9.4% of genes belonged to
301 transferase (PC00220), 5.5% of genes belonged to cytoskeletal protein (PC00085), and 5.0% of genes
302 belonged to transporter (PC00227) of protein classes.

303 Pathway enrichment analysis using the DEGs identified the following enriched pathways: pentose
304 phosphate pathway (11 genes), carbon metabolism (30 genes), p53 signaling pathway (22 genes),
305 apoptosis (32 genes), pyrimidine metabolism (27 genes), ubiquitin-proteasome pathway (15 genes),
306 TGFβ signaling pathway (37 genes), and glycolysis (6 genes) (Figure 6C).

307 **Table 1.** List of Pentose phosphate pathway genes, and antioxidant genes along with ensembl, gene
308 symbol, gene name logFC, p-values in RNA seq data analysis.

Pentose phosphate pathway				
Ensembl	**Gene Symbol**	**Gene Name**	**logFC**	**p-value**
ENST00000566012	ALDOA	aldolase, fructose-bisphosphate A	-2.70711	0.000159
ENST00000226253	ALDOC	aldolase, fructose-bisphosphate C	-8.29613	3.54E-06
ENST00000533447	DERA	deoxyribose-phosphate aldolase	3.07566	0.000305
ENSG00000160211	G6PD*	glucose-6-phosphate dehydrogenase	6.20824	1.08E-12
ENST00000486393	GLYCTK	glycerate kinase	-7.43140	0.000164
ENST00000588991	GPI	glucose-6-phosphate isomerase	-7.36468	0.000217
ENST00000397961	PFKL	phosphofructokinase, liver type	7.15971	0.000530
ENST00000551339	PFKM	phosphofructokinase, muscle	-10.6579	2.97E-12
ENST00000594761	PGLS	6-phosphogluconolactonase	7.41946	0.000217
ENST00000372419	PRPS1	phosphoribosyl pyrophosphate synthetase 1	-8.25372	4.28E-06
ENST00000429907	RPE	ribulose-5-phosphate-3-epimerase	7.75075	4.53E-05

309 * G6PD logFC values and p-value was consistent with western blot analysis results.

310 **Table 2.** List of Pentose phosphate pathway genes and antioxidant genes along with ensembl, gene
311 symbol, gene name logFC, p-values in RNA seq data analysis.

Ensembl	**Gene Symbol**	**Gene Name**	**logFC**	**p-value**
ENST00000544168	AKT1	AKT serine/threonine kinase 1	-2.365428775	0.0023003
ENST00000474136	APP	amyloid beta precursor protein	-11.37328742	2.77E-14
ENST00000393468	CAV1	caveolin 1	-2.252194366	0.00204467
ENST00000542367	CCND1	cyclin D1	3.391893687	5.44E-06
ENST00000405375	CDKN1A	cyclin dependent kinase inhibitor 1A	-8.013577331	1.45E-05
ENST00000509337	DAB2	DAB2, clathrin adaptor protein	9.945707367	2.78E-10
ENST00000526145	ETS1	ETS proto-oncogene 1, transcription factor	3.384794454	0.00455057
ENST00000474036	FN1	fibronectin 1	3.02069906	0.00472911
ENST00000428704	HDAC1	histone deacetylase 1	-7.143753011	0.00053040
ENST00000560629	ITGB3	integrin subunit beta 3	-7.614824773	9.64E-05
ENST00000200181	ITGB4	integrin subunit beta 4	7.294499935	0.00039082

Preprints (www.preprints.org) | NOT PEER-REVIEWED | Posted: 10 July 2019 doi:10.20944/preprints201907.0140.v1

ENST00000535335	KLF11	Kruppel like factor 11	8.042834182	1.17E-05
ENST00000333611	LIMK2	LIM domain kinase 2	8.171648208	6.32E-06
ENST00000393362	MAPK9	mitogen-activated protein kinase 9	-2.849607483	0.00291167
ENST00000504921	MEF2C	myocyte enhancer factor 2C	-8.39414907	2.05E-06
ENST00000318493	MET	MET proto-oncogene, receptor tyrosine kinase	-8.922971532	1.28E-07
ENST00000504387	NEDD9	neural precursor cell expressed, developmentally down-regulated 9	2.177612821	0.00196987
ENST00000567606	PML	promyelocytic leukemia	-9.040096253	5.90E-08
ENST00000296446	PRKAR2A	protein kinase cAMP-dependent type II regulatory subunit alpha	-8.667581639	4.66E-07
ENST00000521791	PTK2	protein tyrosine kinase 2	-4.161512038	0.00133434
ENST00000423275	RAF1	Raf-1 proto-oncogene, serine/threonine kinase	-9.032436585	6.69E-08
ENST00000635540	ROCK1	Rho associated coiled-coil containing protein kinase 1	-10.50374244	8.23E-12
ENST00000368453	SHC1	SHC adaptor protein 1	-6.232971845	1.30E-10
ENST00000402690	SMAD2	SMAD family member 2	-2.662985055	0.00074433
ENST00000398417	SMAD4	SMAD family member 4	-7.777534707	4.53E-05
ENST00000555761	SNW1	SNW domain containing 1	-7.431403503	0.00016479
ENST00000426016	SOS1	SOS Ras/Rac guanine nucleotide exchange factor 1	-8.32564549	2.94E-06
ENST00000389980	SPTBN1	spectrin beta, non-erythrocytic 1	11.65618569	4.17E-15
ENST00000025399	STRAP	serine/threonine kinase receptor associated protein	-7.294735531	0.00029061
ENST00000567066	TGFB1I1	transforming growth factor beta 1 induced transcript 1	8.564730191	8.76E-07
ENST00000525962	TGFBR3	transforming growth factor beta receptor 3	8.212151204	5.19E-06
ENST00000576106	TRAP1	TNF receptor associated protein 1	-3.530510601	0.00019337
ENST00000367450	UCHL5	ubiquitin C-terminal hydrolase L5	-7.556237722	0.00012556
ENST00000265428	WWP1	WW domain containing E3 ubiquitin protein ligase 1	-9.115939287	4.09E-08
ENST00000615667	YAP1	Yes associated protein 1	8.212151204	5.19E-06
ENST00000542815	ZEB1	zinc finger E-box binding homeobox 1	9.268512943	1.64E-08
ENST00000392861	ZEB2	zinc finger E-box binding homeobox 2	4.55061543	0.00038525

312

313

Preprints (www.preprints.org) | NOT PEER-REVIEWED | Posted: 10 July 2019 doi:10.20944/preprints201907.0140.v1

Table 3. List of cell adhesion and antioxidant genes along with ensembl, gene symbol, gene name logFC, p-values in RNA seq data analysis.

Ensembl	Gene Symbol	Gene Name	logFC	p-value
ENST00000553755	LGALS3	galectin 3	8.399184809	2.05E-06
ENST00000619499	FBN2	fibrillin 2	7.294499935	0.00039082
ENST00000559133	FBN1	fibrillin 1	7.294735531	0.00029061
ENST00000599225	LTBP4	latent transforming growth factor beta binding protein 4	7.556237722	0.00012556
ENST00000258733	GPNMB	glycoprotein nmb	7.777534707	4.53E-05
ENST00000454637	CELSR1	cadherin EGF LAG seven-pass G-type receptor 1	7.901380997	2.25E-05
ENST00000200181	ITGB4	integrin subunit beta 4	7.294499935	0.00039082
ENST00000377996	TMEM8B	transmembrane protein 8B	7.629619087	7.45E-05
ENST00000542878	MFGE8	milk fat globule-EGF factor 8 protein	9.623631113	1.90E-09
ENST00000560629	ITGB3	integrin subunit beta 3	7.614824773	9.64E-05
ENST00000403076	SDC1	syndecan 1	7.061890851	0.00072685
ENST00000360134	MAGED4B	MAGE family member D4B	9.175540117	2.87E-08
ENST00000514554	TGFBI	transforming growth factor beta induced	7.744535809	4.53E-05
ENST00000474729	MPZL1	myelin protein zero like 1	7.495170406	0.00016479
ENST00000397857	ITGB2	integrin subunit beta 2	8.013577331	1.45E-05
ENST00000439986	CCBE1	collagen and calcium binding EGF domains 1	5.657885256	2.14E-06
ENST00000218439	MAGED2	MAGE family member D2	2.285685523	0.00330434
ENST00000539168	CDH5*	VE-cadherin	9.90760	3.47E-10
ENST00000262746	PRDX1	peroxiredoxin 1	7.453892	0.000217
ENSG00000165672	PRDX3	peroxiredoxin 3	7.265215	0.000727
ENST00000470017	PRDX6	peroxiredoxin 6	8.171648	0.001060

* CDH5 (VE-cadherin) logFC values and p-value was consistent with western blot analysis results.

The functional enrichment results revealed genes mainly involved in the pentose phosphate pathway (Table 1), TGFβ signaling pathway (Table 2), as well as cell adhesion and antioxidant genes that we have identified and tabulated (Table 3); these are all up-regulated in PlGF ab treated conditions compared with the control. These results suggested that most of the genes involved in the TGFβ signaling pathway might have a beneficial role in treatment of diabetic retinopathy.

3.2.2 Pathway-focused gene interaction network analysis

We performed the gene-gene network analysis of genes within each pathway using the STRING tool (https://string-db.org/). Given our previous observation of the effect of high glucose on the expression of PIGF, here we focused our analysis on the genes identified to be involved in the pentose phosphate pathway. All the of 11 genes that were identified above were used for the gene-interaction analysis, with the human genome as the background. Interestingly from the analysis, G6PD, which is a gene that we previously found to be modulated under high glucose, was shown to interact with genes

 doi:10.20944/preprints201907.0140.v1

such as PFKM, ALDOA, RPE, PGLS, and ALDOC (Suppl. Figure 1A). The carbon metabolism pathway has 30 nodes, 195 edges, a 13 average node degree, 0.749 avg. local clustering coefficient, and 9 expected number of edges with a PPI enrichment p-value < 1.0e-16 (Suppl. Figure 1B). The p53 signaling pathway has 22 nodes, 111 edges, a 10.1 average node degree, 0.75 avg. local clustering coefficient and 15 expected number of edges with a PPI enrichment p-value < 1.0e-16 (Suppl. Figure1C). The apoptosis pathway has 31 nodes, 207 edges, a 13.4 average node degree, 0.728 avg. local clustering coefficient, and 30 expected number of edges with a PPI enrichment p-value < 1.0e-16 (Suppl. Figure1D). The Pyrimidine metabolism pathway has 27 nodes, 159 edges, 11.8 average node degree, 0.715 avg. local clustering coefficient, and 12 expected number of edges with a PPI enrichment p-value < 1.0e-16 (Suppl. Figure2A). The ubiquitin-mediated proteolysis pathway has 15 nodes, 56 edges, a 7.47 average node degree, 0.717 avg. local clustering coefficient, and 8 expected number of edges with a PPI enrichment p-value < 1.0e-16 (Suppl. Figure2B). The TGFβ signaling pathway has 37 nodes, 162 edges, an 8.76 average node degree, 0.606 avg. local clustering coefficient, and 47 expected number of edges with a PPI enrichment p-value < 1.0e-16 (Suppl. Figure2C). The glycolysis pathway has 6 nodes, 15 edges, a 5.0 average node degree, 1 avg. local clustering coefficient, and 1 expected number of edges with a PPI enrichment p-value < 1.0e-16 (Suppl. Figure2D). The results revealed that all pathway genes interact with each other directly or indirectly, except the EIF2S1 gene in the apoptosis pathway.

3.2.3 Gene-interaction network analysis of genes within the pentose phosphate pathway

Preprints (www.preprints.org) | NOT PEER-REVIEWED | Posted: 10 July 2019 doi:10.20944/preprints201907.0140.v1

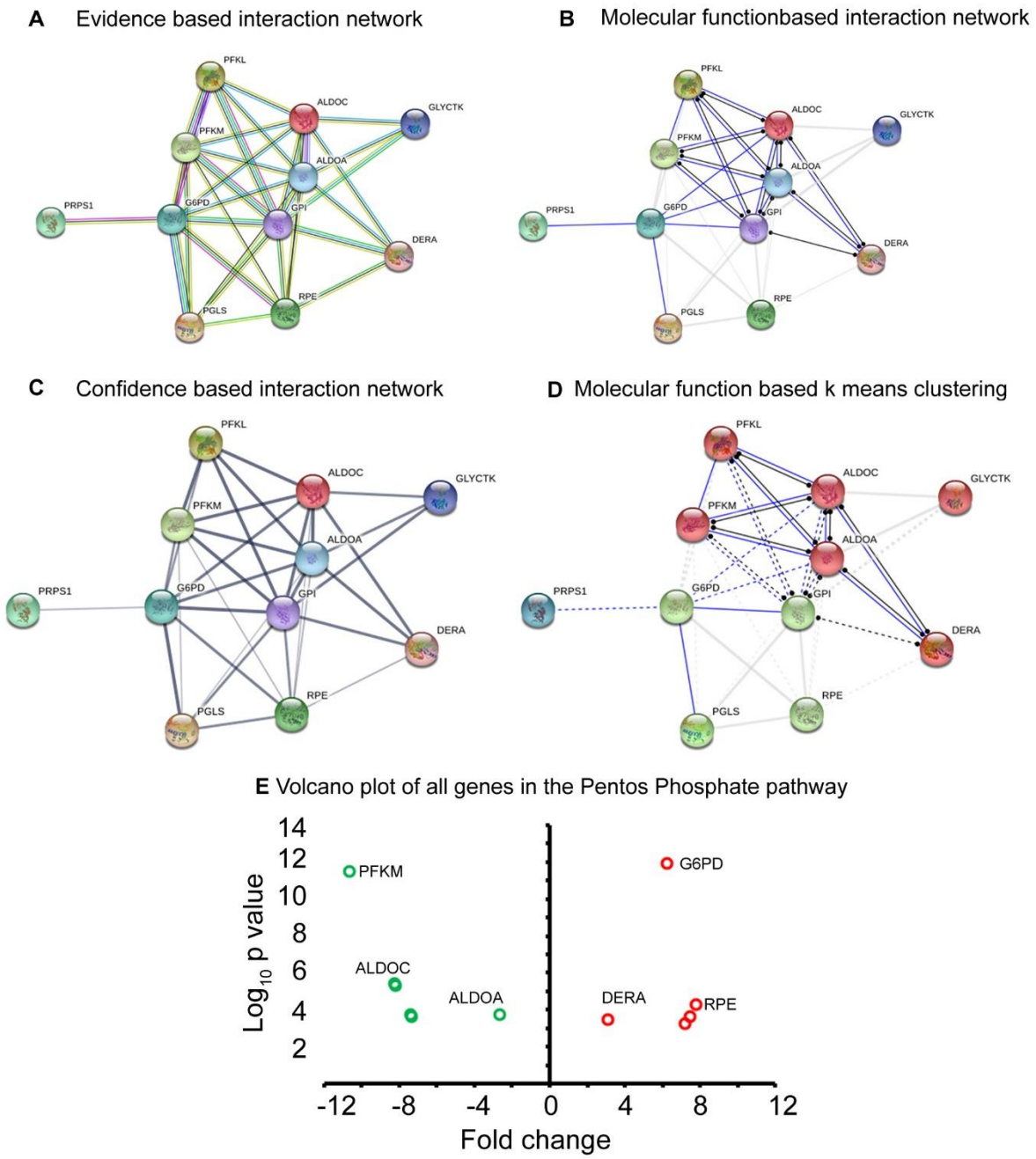

Figure 7. Interaction network analysis of genes involved in the pentose phosphate pathway. **A** is the evidence-based interaction network analysis, **B** is the molecular function-based interaction network analysis, **C** is the confidence-based interaction network analysis, and **D** is a k means cluster analysis of the genes. The grey arrow in A-D points to G6PD protein. **E** is a volcano plot of fold change and p-value of all pentose phosphate pathway genes.

Given our previous observation about the effect of PIGF on glucose-6-phosphate dehydrogenase (G6PD) and the antioxidant system (manuscript under review), here we focused our analysis on the genes identified in the pentose phosphate pathway. All of the 11 genes that were identified above (under pathway enrichment analysis) were used for the gene-interaction analysis, with the human genome as the background using STRING (https://string-db.org/). Evidenced-based analysis of the genes showed that all the genes were inter-connected, and ALDOC was the query protein and first shell of interactors. Interestingly, G6PD, a gene that we previously found to be modulated under high glucose and by PlGF, was shown to interact with many genes such as PFKM, ALDOA, RPE, PGLS, and ALDOC (Figure 7A). An interaction analysis based on molecular action was also performed to gain insights into how these genes affect each other, and the results reveal that G6PD binds directly

Preprints (www.preprints.org) | NOT PEER-REVIEWED | Posted: 10 July 2019 doi:10.20944/preprints201907.0140.v1

with PRPS1, PGLS, GPI, ALDOA, and ALDOC (Figure 7B). Based on confidence analysis, G6PD showed the highest interaction with GPI, RPE, PGLS, ALDOA, ALDOC, and high interaction with PRPS (Figure 7C). Reactome pathway analysis revealed that glycolysis and TP53 regulates metabolic genes and are among the enriched pathways, with FDR of 1.30e-09 and 0.0023, respectively (Supp Table 1.). In addition, G6PD was involved in three of the 6 enriched Reactome pathways. Clustering of the 11 genes involved in the pentose phosphate pathway revealed two distinctive clusters. In one cluster genes, G6PD, PGLS, RPE, and GP1 were grouped, while PFKL, PFKM, ALDOC, ALDOA, DERA, and GLYCTK clustered together. PRPS1 was the only gene that did not cluster with any of the above (Figure 7D).

3.2.4 Gene-interaction network analysis of genes within the TGF-β signaling pathway

TGF-β signaling has been implicated in the pathophysiology of DR, for instance during the thickening of the capillary basal lamina, mediated via pericytes. Here, we performed an in-depth analysis of the genes identified from the pathway analysis involved in TGF-β signaling, in order to understand how these genes interact with each other in modulating cell behavior after antibody-mediated inhibition of PlGF in vitro. The evidence-based analysis identified integrin beta-4; (ITGB4) as the query protein, and the first shell of interactors (Figure 8A), a protein thought to play a role in the hemidesmosome of epithelial cells. Analysis based on molecular function revealed that ITGB4 binds directly to PTK2, MET, ITGB3, CAV1, and SHC1, which in turn inhibit ZEB1 (Figure 8B), and a confidence-based interaction analysis revealed that ITGB4 binds strongly with the above proteins (Figure 8C). Cluster analysis of all the genes involved in the TGF-β pathway revealed three distinctive clusters of genes; Cluster 1 (green), cluster 2 (red), and cluster 3 (Dark cyan) (Figure 8D).

Preprints (www.preprints.org) | NOT PEER-REVIEWED | Posted: 10 July 2019 doi:10.20944/preprints201907.0140.v1

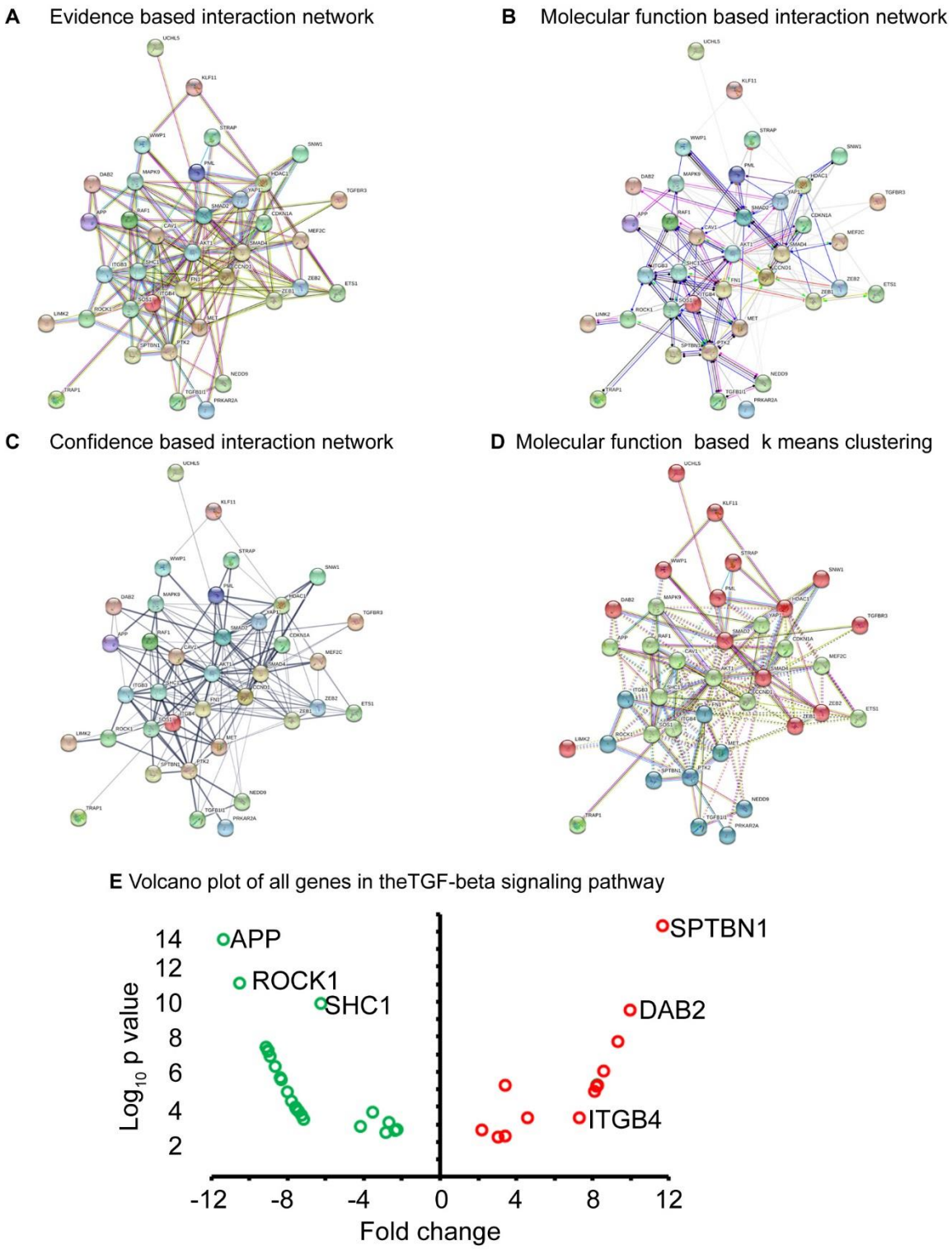

Figure 8. Interaction network analysis of genes involved in the TGF-beta signaling pathway. **A** is the evidence-based interaction network analysis, **B** is the molecular function-based interaction network analysis, **C** is the confidence-based interaction network analysis, and **D** is a k means cluster analysis of the genes. **E** is a volcano plot of fold change and p-value of all TGFβ signaling pathway genes.

4. Discussion

 doi:10.20944/preprints201907.0140.v1

The current study has elucidated the transcriptome-wide gene profile of HREC with the presence and the absence of PlGF signaling. The DEGs identified in the PlGF treated group relative to the control were further characterized and annotated for gene ontology and functional enrichment analysis. The downstream genes and pathways regulated by PlGF are potentially involved in the biological functions of PlGF, such as angiogenesis and EC barrier function.

One interesting class of genes are those involved in the TGFβ signaling pathway. The functional enrichment results revealed that the AKT1, APP, CAV1, CCND1, CDKN1A, DAB2, ETS1, FN1, HDAC1, ITGB3, ITGB4, KLF11, LIMK2, MAPK9, MEF2C, MET, NEDD9, PML, PRKAR2A, PTK2, RAF1, ROCK1, SHC1, SMAD2, SMAD4, SNW1, SOS1, SPTBN1, STRAP, TGFB1I1, TGFBR3, TRAP1, UCHL5, WWP1, YAP1, ZEB1, and ZEB2 genes are involved in the TGFβ signaling pathway. TGFβ1 is a signaling protein involved in many processes, including immune system modulation, cell proliferation, cell differentiation, and apoptosis [21]. After activation, TGF-β binds to the type 2 TGF-β receptor, and this interaction leads to recruitment and subsequential phosphorylation of type 1 TGF-β receptor. In turn, the intracellular proteins Smad2 and Smad3 are recruited, and after forming a complex with Smad4, TGF-β translocates into the nucleus, where it activates downstream gene transcription [22].

With regards to BBB (blood brain barrier) permeability, evidence supports that TGFβ1 can directly affect endothelial cell permeability. Behzadian et al., (2001) [23] reported that retinal endothelial cells treated with TGFβ1 were found to increase MMP9 expression, which increased the permeability of these endothelial cells. Our results also suggest that the MMP14 gene is up-regulated and supported the above observations. Previous reports indicate that TGF-β signaling is complex, with autocrine and paracrine signaling reported for multiple cell types, and widespread detection of both receptor and ligand expression [24]. Moreover, recent studies of neuronal morphogenesis in the brain demonstrated that TGF-β signaling is required for both axon formation and migration [25]. Brionne et al., (2003) [26] reported that mice exhibits lacking TGF-β1 show a widespread increase in degeneration of neurons in the brain and prominent microgliosis prior to death. TGF-β1 is a multifunctional growth factor that is a well-established modulator of vascular cells [27]. Previous studies indicated that TGF-β1 is activated upon contact between endothelial and mesenchymal cells and that it mediates a variety of actions associated with vessel maturation including inhibition of EC proliferation and migration, induction of pericyte differentiation, and production of basement membranes [28]. Pericytes and astrocytes may also release TGF-β, which contributes to BBB integrity and function [29]. Recent studies have demonstrated that contact between endothelium cells (ECs) and pericytes or astrocytes leads to TGF-β1 activation (up-regulated), a major determinant of TGF-β1 availability and signaling. [30] Moreover, the loss of retinal pericytes has been speculated to be permissive for the progression of diabetic retinopathy [31]. These explanations suggest that the high number of pericytes in the retina reflects a significant role for constitutive TGF-β1 signaling in the maintenance of retinal microvascular integrity. The above literature reports are well correlated with our findings. Braunger et al., (2013) reported that the TGF-β1 signaling exerts pleiotropic effects on multiple retinal cell types that underlie numerous functions ranging from maintaining retinal neuronal differentiation and survival in the retina [32]. Shen et al., (2011) [33] study demonstrated that TGF-β1 stimulation of both bovine retinal ECs and human BECs increase BBB permeability. Notably, the increased BBB permeability was mediated by tyrosine-phosphorylation of both claudin-5 and VE-cadherin. TGF-β1signaling has been acknowledged as pivotal in the differentiation of vascular smooth muscle cells/pericytes at mid-gestation, as revealed by gene knockout studies on the signal components, including TGF-β1, Tgfbr2, Alk1, Alk5, endoglin, Smad5, and Smad4 [34]. Our findings suggest that the SMAD2 and SMAD4 genes are down-regulated in the TGF-β1signaling pathway. This might have a significant role in dysregulation of the ubiquitin proteasome pathway, angiogenesis pathway, p53 signaling pathway, and apoptosis pathway genes, as well as in up-regulation of the many cell-cell adhesion genes including LGALS3, FBN2, FBN1, LTBP4, GPNMB, CELSR1, ITGB4, TMEM8B, MFGE8, ITGB3, SDC1, MAGED4B, MPZL1, ITGB2, CCBE1, and MAGED2, and increase of the BBB permeability.

 doi:10.20944/preprints201907.0140.v1

The other genes of interest from the pentose phosphate pathway (PPP) and antioxidant defense system, the glycolysis and carbon metabolism genes, play a beneficial role in diabetes-related oxidative damage to retinal cells (diabetic retinopathy). Oxidative stress is caused by an imbalance between the antioxidant defense system and the production of reactive oxygen species (ROS) [35]. G6PD gene plays a key role in regulating carbon flow through the pentose phosphate pathway. Specifically, the enzyme affects the production of the reduced form of the extramitochondrial nicotine adenosine dinucleotide phosphate (NADPH) coenzyme by controlling the conversion from glucose-6-phosphate to 6-phosphogluconate in the pentose phosphate pathway. In red blood cells, defense against oxidative damage is heavily dependent on G6PD activity, which is the only source of NADPH [36]. Our results suggest that the G6PD gene is up-regulated in the PlGF ab treated condition. It stimulates the oxidative branch of PPP to supply cytosolic NADPH to counteract oxidative damage as well as up-regulating antioxidant genes such as Peroxiredoxin (Prdx)1, Prdx3, and Prdx6. Prdxs are a family of highly conserved, low molecular weight (20–30 kDa) thiol peroxidases that scavenge hydrogen peroxide, alkyl hydroperoxides, and peroxynitrite in living cells [37]. Prdxs play a pivotal role in the response of cells to oxidative stress. Moreover, increasing evidence suggests that certain Prdxs also act as redox sensors: under conditions of oxidative stress, hyperoxidation of the Prdx molecule can occur via binding of a second peroxide substrate, resulting in the cellular build-up of Prdx oxidation products and the local accumulation of hydrogen peroxide [38]. In the retina, only Müller cells and astrocytes that play a crucial role in the maintenance of blood-retinal barrier function express Prdx6. Further, decreased Prdx6 has been reported in several disease conditions where the blood-retinal barrier is compromised. These include diabetic retinopathy (DR), exudative age-related macular degeneration (AMD) as well as arterial and venous occlusions [37] [39]. Our previous proteomics studies also reported that PlGF deficiency increases antioxidant and neuroprotective proteins in the diabetic mouse retina [18]. Recent studies on tears from patients with glaucoma have also identified Prdx1 as having a possible involvement in inflammation [40]. Furthermore, apart from their role as antioxidants, the peroxiredoxins can affect a diverse range of biological processes that include cellular proliferation, differentiation, and apoptosis by influencing signal transduction pathways that employ hydrogen peroxide as a secondary messenger [41]. All of the above findings suggest that PRDX1, PRDX3, and PRDX6 play a defending role in oxidative stress PlGF ab treated in a high glucose condition.

5. Conclusions

Our results primarily demonstrated that neutralizing PlGF regulates a variety of gene expressions that are relevant to its pathophysiological functional roles, such as angiogenesis and EC barrier function. Among the most important ones are those genes involved in TGFβ, PPP, and the antioxidant defense system. These newly identified genes may act as target molecules for therapeutic interventions for those patients with DR refractory to the current anti-VEGF therapy.

Author Contributions: conceptualization, H.H. and M.S.S.; methodology, M.S.S. H.H. and L.F.; software, M.S.S..; validation, A.L.; formal analysis, M.S..; investigation, A.L. A.M and M.S.S; resources, H.H.; data curation, H.H.; writing—original draft preparation, M.S.S., H.H., A.L. and A.M.; writing—review and editing, H.H., A.L. and A.M.; visualization, M.S.S., A.L and A.M.; supervision, H.H.; project administration, H.H.; funding acquisition, H.H."

Funding: This research was funded by National Eye Institute, grant number EY027824, and University of Missouri start-up fund.

Acknowledgments: The authors wish to acknowledge the contribution of the Center for Biomedical Informatics (CBMI) University of Missouri (Columbia, MO, USA) for computer application facilities and Mr. Dmitry Rumyancev (Belgorod, Russia) for graphical abstract artwork assets design.

Conflicts of Interest: "The authors declare no conflict of interest."

Appendix A

Preprints (www.preprints.org) | NOT PEER-REVIEWED | Posted: 10 July 2019 doi:10.20944/preprints201907.0140.v1

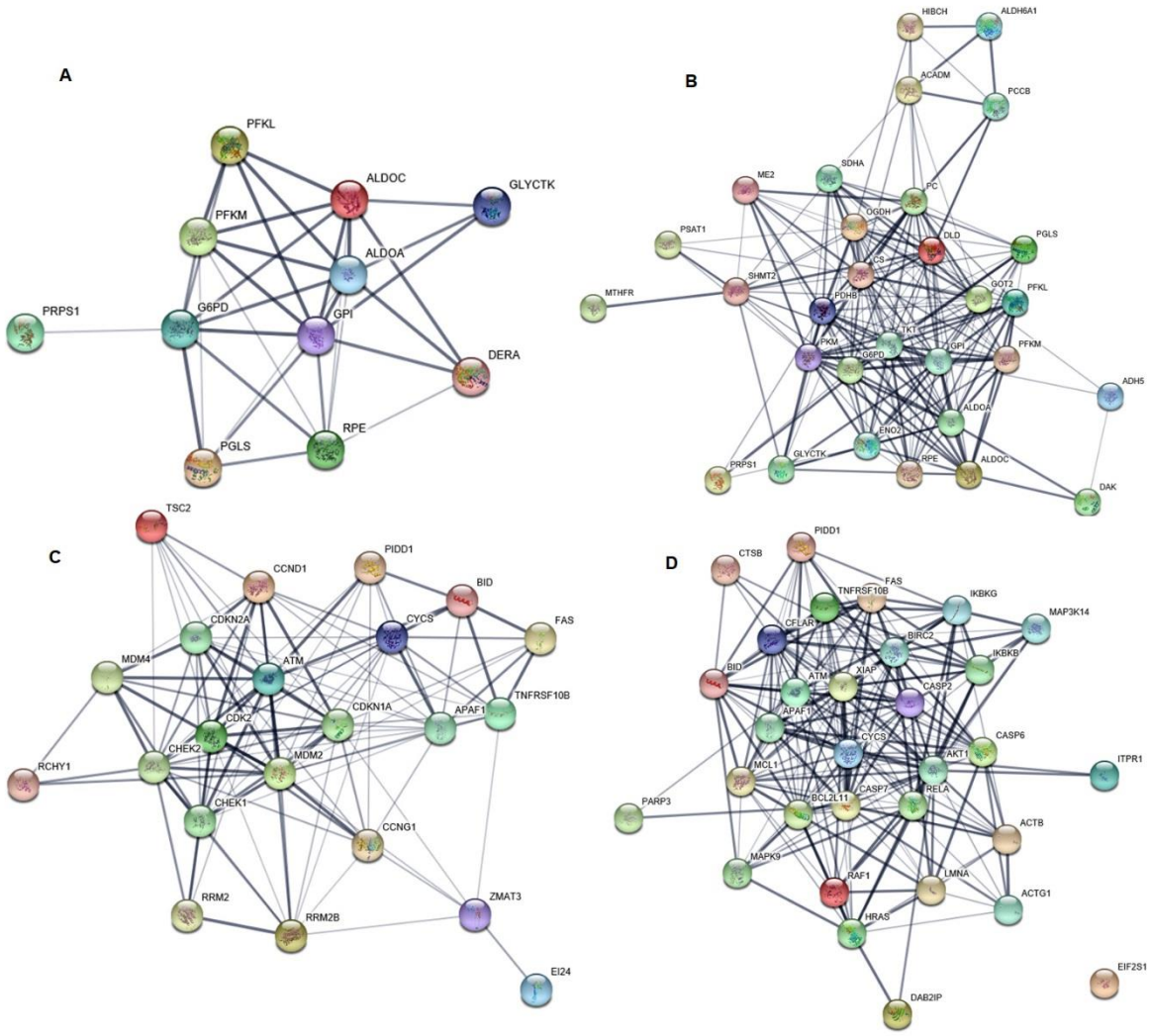

Supplementary Figure 1. The primary gene network is divided into sub-networks. **A**. Pentose phosphate pathway genes sub-network **B**. Carbon metabolism pathway genes sub-network **C**. p53 signaling pathway genes subnetwork. **D**. Apoptosis pathway genes subnetwork.

Preprints (www.preprints.org) | NOT PEER-REVIEWED | Posted: 10 July 2019 doi:10.20944/preprints201907.0140.v1

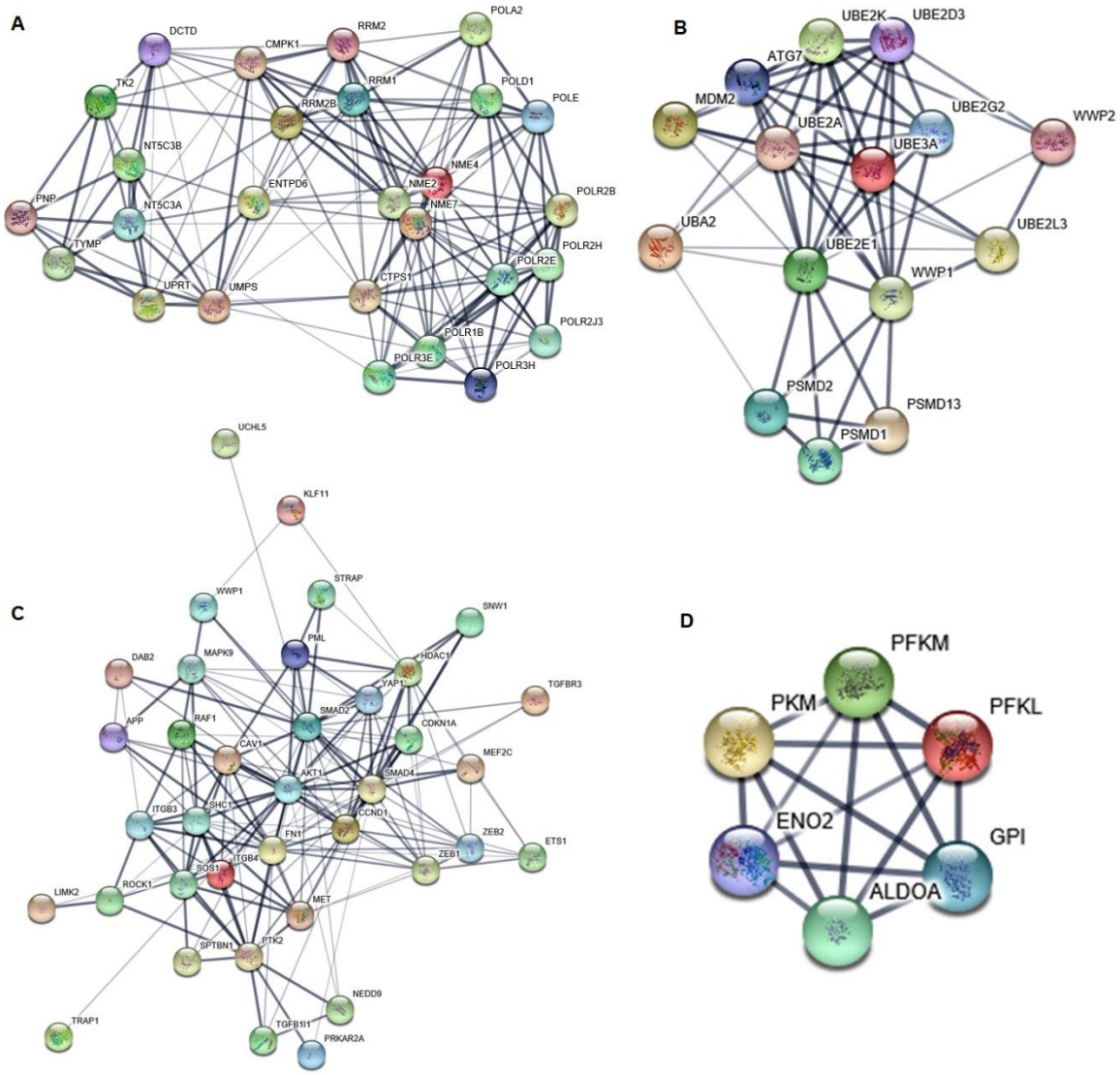

Supplementary Figure 2. The primary gene network is divided into sub-networks. **A**. Pyrimidine metabolism pathway genes sub-network **B**. Ubiquitin-proteasome pathway genes sub-network **C**. TGF-beta signalling pathway genes subnetwork. **D**. Glycolysis pathway genes subnetwork.

 doi:10.20944/preprints201907.0140.v1

References

1. Lee, R.; Wong, T.Y.; Sabanayagam, C. Epidemiology of diabetic retinopathy, diabetic macular edema and related vision loss. *Eye Vis (Lond)* **2015**, *2*, 17.
2. Curtis, T.M.; Gardiner, T.A.; Stitt, A.W. Microvascular lesions of diabetic retinopathy: Clues towards understanding pathogenesis? *Eye (Lond)* **2009**, *23*, 1496-1508.
3. Friedlander, M. Fibrosis and diseases of the eye. *J Clin Invest* **2007**, *117*, 576-586.
4. Elman, M.J.; Aiello, L.P.; Beck, R.W.; Bressler, N.M.; Bressler, S.B.; Edwards, A.R.; Ferris, F.L.; Friedman, S.M.; Glassman, A.R.; Miller, K.M., *et al.* Randomized trial evaluating ranibizumab plus prompt or deferred laser or triamcinolone plus prompt laser for diabetic macular edema. *Ophthalmology* **2010**, *117*, 1064-U1065.
5. Storkebaum, E.; Carmeliet, P. Vegf: A critical player in neurodegeneration. *J Clin Invest* **2004**, *113*, 14-18.
6. Aiello, L.P. Angiogenic pathways in diabetic retinopathy. *New Engl J Med* **2005**, *353*, 839-841.
7. Maglione, D.; Guerriero, V.; Viglietto, G.; Dellibovi, P.; Persico, M.G. Isolation of a human placenta cdna coding for a protein related to the vascular-permeability factor. *Proceedings of the National Academy of Sciences of the United States of America* **1991**, *88*, 9267-9271.
8. Saddala, M.S.; Lennikov, A.; Grab, D.J.; Liu, G.S.; Tang, S.B.; Huang, H. Proteomics reveals ablation of pigf increases antioxidant and neuroprotective proteins in the diabetic mouse retina. *Scientific reports* **2018**, *8*.
9. Ohno-Matsui, K.; Uetama, T.; Yoshida, T.; Hayano, M.; Itoh, T.; Morita, I.; Mochizuki, M. Reduced retinal angiogenesis in mmp-2-deficient mice. *Investigative ophthalmology & visual science* **2003**, *44*, 5370-5375.
10. Autiero, M.; Waltenberger, J.; Communi, D.; Kranz, A.; Moons, L.; Lambrechts, D.; Kroll, J.; Plaisance, S.; De Mol, M.; Bono, F., *et al.* Role of pigf in the intra- and intermolecular cross talk between the vegf receptors flt1 and flk1. *Nature medicine* **2003**, *9*, 936-943.
11. Carmeliet, P.; Moons, L.; Luttun, A.; Vincenti, V.; Compernolle, V.; De Mol, M.; Wu, Y.; Bon, F.; Devy, L.; Beck, H., *et al.* Synergism between vascular endothelial growth factor and placental growth factor contributes to angiogenesis and plasma extravasation in pathological conditions. *Nature medicine* **2001**, *7*, 575-583.
12. Huang, H.; He, J.B.; Johnson, D.; Wei, Y.H.; Liu, Y.; Wang, S.; Lutty, G.A.; Duh, E.J.; Semba, R.D.; Carmeliet, P. Deletion of placental growth factor prevents diabetic retinopathy and is associated with akt activation and hif1 alpha-vegf pathway inhibition (vol 64, pg 200, 2015). *Diabetes* **2015**, *64*, 1067-1067.
13. Giaever, I.; Keese, C.R. Micromotion of mammalian cells measured electrically. *Proceedings of the National Academy of Sciences of the United States of America* **1991**, *88*, 7896-7900.
14. Huang, H.; Shen, J.; Vinores, S.A. Blockade of vegfr1 and 2 suppresses pathological angiogenesis and vascular leakage in the eye. *PLoS One* **2011**, *6*, e21411.
15. Huang, H.; Van de Veire, S.; Dalal, M.; Parlier, R.; Semba, R.D.; Carmeliet, P.; Vinores, S.A. Reduced retinal neovascularization, vascular permeability, and apoptosis in ischemic retinopathy in the absence of prolyl hydroxylase-1 due to the prevention of hyperoxia-induced vascular obliteration. *Investigative ophthalmology & visual science* **2011**, *52*, 7565-7573.
16. Bolger, A.M.; Lohse, M.; Usadel, B. Trimmomatic: A flexible trimmer for illumina sequence data. *Bioinformatics* **2014**, *30*, 2114-2120.

17. Huang, D.W.; Sherman, B.T.; Tan, Q.; Kir, J.; Liu, D.; Bryant, D.; Guo, Y.; Stephens, R.; Baseler, M.W.; Lane, H.C., *et al.* David bioinformatics resources: Expanded annotation database and novel algorithms to better extract biology from large gene lists. *Nucleic Acids Res* **2007**, *35*, W169-175.
18. Saddala, M.S.; Lennikov, A.; Grab, D.J.; Liu, G.S.; Tang, S.; Huang, H. Proteomics reveals ablation of plgf increases antioxidant and neuroprotective proteins in the diabetic mouse retina. *Scientific reports* **2018**, *8*, 16728.
19. Rivals, I.; Personnaz, L.; Taing, L.; Potier, M.C. Enrichment or depletion of a go category within a class of genes: Which test? *Bioinformatics* **2007**, *23*, 401-407.
20. Dennis, G.; Sherman, B.T.; Hosack, D.A.; Yang, J.; Gao, W.; Lane, H.C.; Lempicki, R.A. David: Database for annotation, visualization, and integrated discovery. *Genome biology* **2003**, *4*, R60.
21. Yoshimura, A.; Wakabayashi, Y.; Mori, T. Cellular and molecular basis for the regulation of inflammation by tgf-beta. *Journal of biochemistry* **2010**, *147*, 781-792.
22. Derynck, R.; Zhang, Y.E. Smad-dependent and smad-independent pathways in tgf-beta family signalling. *Nature* **2003**, *425*, 577-584.
23. Behzadian, M.A.; Wang, X.L.; Windsor, L.J.; Ghaly, N.; Caldwell, R.B. Tgf-beta increases retinal endothelial cell permeability by increasing mmp-9: Possible role of glial cells in endothelial barrier function. *Investigative ophthalmology & visual science* **2001**, *42*, 853-859.
24. Close, J.L.; Gumuscu, B.; Reh, T.A. Retinal neurons regulate proliferation of postnatal progenitors and muller glia in the rat retina via tgf beta signaling. *Development* **2005**, *132*, 3015-3026.
25. Yi, J.J.; Barnes, A.P.; Hand, R.; Polleux, F.; Ehlers, M.D. Tgf-beta signaling specifies axons during brain development. *Cell* **2010**, *142*, 144-157.
26. Brionne, T.C.; Tesseur, I.; Masliah, E.; Wyss-Coray, T. Loss of tgf-beta 1 leads to increased neuronal cell death and microgliosis in mouse brain. *Neuron* **2003**, *40*, 1133-1145.
27. ten Dijke, P.; Arthur, H.M. Extracellular control of tgfbeta signalling in vascular development and disease. *Nature reviews. Molecular cell biology* **2007**, *8*, 857-869.
28. Neubauer, K.; Kruger, M.; Quondamatteo, F.; Knittel, T.; Saile, B.; Ramadori, G. Transforming growth factor-beta1 stimulates the synthesis of basement membrane proteins laminin, collagen type iv and entactin in rat liver sinusoidal endothelial cells. *Journal of hepatology* **1999**, *31*, 692-702.
29. Obermeier, B.; Daneman, R.; Ransohoff, R.M. Development, maintenance and disruption of the blood-brain barrier. *Nature medicine* **2013**, *19*, 1584-1596.
30. Song, L.; Yan, Y.; Marzano, M.; Li, Y. Studying heterotypic cell¯cell interactions in the human brain using pluripotent stem cell models for neurodegeneration. *Cells* **2019**, *8*, 299.
31. Hammes, H.P. Pericytes and the pathogenesis of diabetic retinopathy. *Horm Metab Res* **2005**, *37 Suppl 1*, 39-43.
32. Braunger, B.M.; Pielmeier, S.; Demmer, C.; Landstorfer, V.; Kawall, D.; Abramov, N.; Leibinger, M.; Kleiter, I.; Fischer, D.; Jagle, H., *et al.* Tgf-beta signaling protects retinal neurons from programmed cell death during the development of the mammalian eye. *J Neurosci* **2013**, *33*, 14246-14258.
33. Shen, W.; Li, S.; Chung, S.H.; Zhu, L.; Stayt, J.; Su, T.; Couraud, P.O.; Romero, I.A.; Weksler, B.; Gillies, M.C. Tyrosine phosphorylation of ve-cadherin and claudin-5 is associated with tgf-beta1-induced permeability of centrally derived vascular endothelium. *European journal of cell biology* **2011**, *90*, 323-332.
34. Lan, Y.; Liu, B.; Yao, H.; Li, F.; Weng, T.; Yang, G.; Li, W.; Cheng, X.; Mao, N.; Yang, X. Essential role of endothelial smad4 in vascular remodeling and integrity. *Molecular and cellular biology* **2007**, *27*, 7683-7692.

35. Masuda, T.; Shimazawa, M.; Hara, H. Retinal diseases associated with oxidative stress and the effects of a free radical scavenger (edaravone). *Oxidative medicine and cellular longevity* **2017**, *2017*, 9208489.
36. Pinna, A.; Carru, C.; Solinas, G.; Zinellu, A.; Carta, F. Glucose-6-phosphate dehydrogenase deficiency in retinal vein occlusion. *Investigative ophthalmology & visual science* **2007**, *48*, 2747-2752.
37. Chidlow, G.; Wood, J.P.; Knoops, B.; Casson, R.J. Expression and distribution of peroxiredoxins in the retina and optic nerve. *Brain structure & function* **2016**, *221*, 3903-3925.
38. Rhee, S.G.; Woo, H.A. Multiple functions of peroxiredoxins: Peroxidases, sensors and regulators of the intracellular messenger h(2)o(2), and protein chaperones. *Antioxid Redox Signal* **2011**, *15*, 781-794.
39. Saddala, M.S.; Lennikov, A.; Mukwaya, A.; Fan, L.; Hu, Z.; Huang, H. Transcriptome-wide analysis of differentially expressed chemokine receptors, snps, and ssrs in the age-related macular degeneration. *Human genomics* **2019**, *13*, 15.
40. Pieragostino, D.; Agnifili, L.; Fasanella, V.; D'Aguanno, S.; Mastropasqua, R.; Di Ilio, C.; Sacchetta, P.; Urbani, A.; Del Boccio, P. Shotgun proteomics reveals specific modulated protein patterns in tears of patients with primary open angle glaucoma naive to therapy. *Molecular bioSystems* **2013**, *9*, 1108-1116.
41. Immenschuh, S.; Baumgart-Vogt, E. Peroxiredoxins, oxidative stress, and cell proliferation. *Antioxid Redox Signal* **2005**, *7*, 768-777.